Applied Environmental Research
- RESEARCH FOR SUSTAINABLE PLANET -

Research Article

Effect of Operating Parameters on Photocatalytic Treatment of Synthetic Wastewater Using $CaTiO_3$

Shilpa Mishra[1,2,*], Rekha Dom[3], Baranidharan Sundaram[1,*]

[1] *Department of Civil Engineering, National Institute of Technology AP, Tadepalligudem, A.P., India*
[2] *Department of Civil Engineering, Maturi Venkata Subba Rao (MVSR) Engineering College, Hyderabad, India*
[3] *Department of Applied Sciences and Humanities, Maturi Venkata Subba Rao (MVSR) Engineering College, Hyderabad, India*

*Correspondence Email: shilpa_civil@mvsrec.edu.in, baranis@nitandhra.ac.in

Abstract

Photocatalysis is thought to be a long-term, environmentally friendly, economically feasible, and promising technique for treating wastewater. The development of semiconductor nanoparticles has generated a great deal of interest in the treatment of wastewater. To break down complex contaminants found in wastewater into simpler compounds, including H_2O and CO_2, several UV/visible light excitable nanomaterials have been explored as photocatalysts. Their effectiveness can be managed by adjusting several reaction-related parameters like the intensity of light, irradiance time, pH, catalyst dose, temperature, doping, etc. The performance of the photocatalyst in the photodegradation of contaminants is greatly affected by these parameters. The main goal of this study is to find the best operational parameters and their impact on the photocatalytic treatment of synthetic wastewater using calcium titanate ($CaTiO_3$) nanoparticles. For this purpose, sol-gel synthesized $CaTiO_3$ with a band gap of 3.57 eV was used. The size of the synthesized nanoparticles is smaller than 47.62 nm. The results of photocatalytic treatment of synthetic wastewater demonstrate that $CaTiO_3$ exhibits its best photocatalytic performance at 33 W UV light, pH 6.0, and 3.33 g L^{-1} $CaTiO_3$ dose with 8 hours of irradiation time. With chemical oxygen demand (COD) concentrations varying from 700 to 40000 mg L^{-1} at the initial stages, the percentage of COD removal under these conditions was 100% to 77%.

ARTICLE HISTORY

Received: 21 Nov. 2023
Accepted: 28 May 2024
Published: 9 Jul. 2024

KEYWORDS

Calcium titanate;
Parameters;
Photocatalysis;
Wastewater;
Nanoparticle

Introduction

An enormous amount of waste is generated due to the rapid growth in population, urbanization, and industrialization. High quantities of inorganic and organic contaminants are present in this waste, which is extremely harmful to the environment [1]. If it is not adequately collected, processed, and disposed of, it can reach water bodies, making it one of the principal causes of pollution in both surface and groundwater [1]. Additionally, the issue was made worse as the pollution of natural water resources worsened because untreated effluent from several industries was frequently discharged into water bodies. Drinking and using contaminated water is harmful to human health and can cause an outbreak of waterborne diseases [2].

Industrial effluents and contaminated water should be appropriately treated before being released into water bodies to avoid the negative impact of water pollution. Several processes are used to treat wastewater before it is released into water bodies, including biological treatment, physical and chemical treatment, coagulation-flocculation, membrane filtration, reverse osmosis, ion exchange, electrolysis, adsorption, and photocatalysis. Each method has its benefits as well as drawbacks, such as the development of secondary waste, sludge, high maintenance costs, membrane fouling, etc. [1, 3–5]. The biological process's target contaminants are suspended

https://doi.org/10.35762/AER.2024031

solids. However, refractory compounds and excess biomass inhibit its effectiveness [6]. Numerous physio-chemical processes, including ion exchange, chemical precipitation, adsorption, oxidation, stripping, and coagulation-flocculation, are appropriate for a variety of contaminants, including suspended solids, heavy metals, NH_3-N, and organic compounds. Their primary drawbacks include high cost, carbon fouling, sludge production, and the requirement of post-treatment subsequently [3, 7]. Membrane filtration has several limitations, including membrane fouling, high cost, and frequent maintenance [8]. Currently, one of the most widely utilized techniques for eliminating a variety of contaminants, including heavy metals, organic, and inorganic compounds, is the advanced oxidation process. Its biggest disadvantage, however, is the high cost of treatment because it requires continuous use of costly chemicals to produce oxidizing radicals, which degrade contaminants [9]. Photocatalytic treatment is one of the most important and cost-effective ways to remove contaminants from wastewater using semiconductor nanoparticles and UV, Visible, or solar light sources. The same nanoparticle can be regenerated and used again without significantly compromising its ability to treat wastewater. However, there is little concern over the dependency of treatment performance on various operational parameters and electron-hole pair recombination [1, 10]. To better understand the efficacy of any treatment process, every operating parameter should be kept under review [11–14].

TiO_2 or Ti-based nanoparticles are the most studied and often used semiconductor nano photocatalyst for wastewater treatment. Numerous studies [15–18] suggest that $CaTiO_3$ could be a viable substitute for TiO_2 in wastewater treatment because it is simple to synthesize using a variety of nanoparticle synthesis techniques, and it can be doped by numerous elements either at Ca or Ti site to reduce electron-hole pair recombination and create oxygen vacancies, which enhance photocatalytic performance, photostability, resistance to photo corrosion, etc. [15–18].

The application of $CaTiO_3$ for the photocatalytic treatment of wastewater with a high initial COD concentration has not yet been covered in any published articles. Recent research [19–32] has concentrated on $CaTiO_3$ photocatalytic applications, but the majority of investigations are concentrated on dye removal from simulated dye solutions. According to a review of the literature [19–28], the photocatalytic performance of $CaTiO_3$ depends on several factors. Some of the important factors that affect its photocatalytic performance are pH, light intensity, irradiation time, catalyst dose, initial concentration of pollutant, calcination temperature (CT), and presence of scavengers as well as oxidants. The removal rate increases as pH increases to an optimal value; beyond that, pH increases further either causes the removal rate to decrease or does not significantly improve. The irradiation time and catalyst dose also showed similar trends. The removal rate increases with increasing light intensity. Because fewer active sites on the catalyst surface are available for the degradation of pollutants with all other parameters keeping unchanged, the removal rate drops as the initial concentration of the pollutant increases. Scavengers reduce photocatalytic performance by reducing the number of electron-hole pairs available for pollutant degradation during the photocatalytic process. However, the presence of an oxidant during the photocatalytic process improves the rate of photocatalytic removal because there are more electron-hole pairs available for the photocatalytic degradation of pollutants.

This research focuses on the efficiency of $CaTiO_3$ as a photocatalytic for the treatment of high COD synthetic wastewater as well as the effects of various operating parameters on photocatalytic treatment, including light intensity, irradiance time, pH, catalyst dose, calcination temperature, initial contaminant concentration, reaction temperature, oxidant and radical scavengers. This will assist researchers in establishing the ideal conditions for the photocatalytic degradation of wastewater such as industrial effluents and landfill leachate using $CaTiO_3$ in future investigations.

Materials and methods

1) Chemicals and reagents

The main consumables and instruments used in this experimental study were solid calcium nitrate tetrahydrate ($Ca(NO_3)_2{\cdot}4H_2O$) from Sigma-Aldrich with 99% purity, tetra butyl titanate (TBT) with 97% purity from Sigma-Aldrich, ammonium metavanadate (NH_4VO_3-SD Fine Chem Limited, 99% purity), Copper Nitrate ($Cu(NO_3)_2{\cdot}4H_2O$, SD Fine Chem Limited, 99% purity), Ferric Nitrate ($Fe(NO_3)_3{\cdot}9H_2O$, SD Fine Chem Limited, 98% purity), citric acid, anhydrous ethanol, peptone, tryptone, NaCl, Na_2SO_4, $CaCl_2{\cdot}2H_2O$, $FeCl_2{\cdot}2H_2O$, $MgCl_2{\cdot}6H_2O$, and K_2HPO_4. Analytical grade consumables were all used exactly as they were, without any additional purification.

2) Instruments and characterization

500 mL beaker, 100 mL measuring jar, 5 mL pipettes, Philips 11W UV lamp, Nexqua RO UV adaptor choke with input 240V and output power 11 W, analytical balance, Remi 2L magnetic stirrer with hot plate 2MLH, 500 mm × 500 mm × 550 mm self-designed photoreactor.

The X-ray diffraction (XRD) method was used to identify the material's crystalline phase. The X'Pert3 Powder X-ray diffraction systems from Malvern Panalytical were used to take XRD patterns. They were run at 45kV and 40mA and used Cu-Kα radiation (λ= 1.5406 Å). With a step size of 2θ and a scan rate of 0.012° per second, the output data were captured within the range of 10.0016° 2θ < 90.0166°, with an increment of 0.0130°. Utilizing the FESEM (Field Emission Scanning Electron Microscopy) and EDX (Energy-dispersive X-ray spectroscopy) methods, the structure and composition of every component in the nanoparticle's surface layer were investigated at a 20 kV accelerating voltage. TEM (Transmission Electron Microscopy) with JEM 1400 Flash from Jeol India Pvt. Ltd was used to measure the size and shape of the nanoparticles. A PG Instrument Limited T90+ double-beam UV-visible spectrophotometer operating at room temperature and covering the wavelength range of 190 –900 nm was used to capture the optical absorbance spectra.

3) Synthesis of $CaTiO_3$

Synthesis of $CaTiO_3$ was performed using the sol-gel method. Drop by drop, 3.4 mL of TBT was dissolved in 30 mL of anhydrous ethanol while stirring constantly. 4.202 g of citric acid was mixed with the TBT solution as a chelating agent. As a calcium percussor, a solid $Ca(NO_3)_2{\cdot}4H_2O$ (2.362 g) was employed. To create the xerogel, the combined solution was magnetically stirred for 1.5 h at 50 °C. After that, it was dried at 80 °C for 12 hours. Following this, the xerogel was calcined at 600 °C for 3 h to form $CaTiO_3$ nanoparticles.

4) Synthesis of doped-$CaTiO_3$

Using the sol-gel process, V-doped $CaTiO_3$ nanoparticles were synthesized. Dropwise dissolution of TBT (Sigma-Aldrich, 98% purity) was added in 30 mL of anhydrous ethanol, with stirring. As a chelating agent, citric acid was used, and the calcium precursor was solid Calcium Nitrate Tetrahydrate (Molychem, 97% purity). Required mol% of ammonium metavanadate (NH_4VO_3-SD Fine Chem Limited, 99% purity) as vanadium precursors, was added to it. To create the xerogel, the combined solution was magnetically stirred for 90 min at 50 °C. It was then dried in an oven for 12 h at 80 °C. Following that, the resultant xerogel was calcined in a furnace for 3 h at 600 °C.

Using 0.295 g of ferric nitrate ($Fe(NO_3)_3{\cdot}9H_2O$, SD Fine Chem Limited, 98% purity) and 0.175 g of copper nitrate ($Cu(NO_3)_2{\cdot}4H_2O$, SD Fine Chem Limited, 99% purity) as the Fe and Cu precursors, respectively, the same procedure was performed to synthesize Fe and Cu-doped $CaTiO_3$ via sol-gel process at calcination temperature of 600 °C.

5) Preparation of synthetic wastewater

The methodology used in this study to produce synthetic wastewater which mimics sewage treatment plant effluent, industrial effluent, and landfill leachate in terms of COD was adapted from previous studies [33–35]. The synthetic wastewater required for this investigation is created in the laboratory using 1 L tap water, 256.55 mg L^{-1} of peptone, 354.24 mg L^{-1} of tryptone, 407.40 mg L^{-1} of NaCl, 44.60 mg L^{-1} of Na_2SO_4, 3.70 mg L^{-1} of $CaCl_2{\cdot}2H_2O$, 3.70 mg L^{-1} of $FeCl_2{\cdot}2H_2O$, 3.70 mg L^{-1} of $MgCl_2{\cdot}6H_2O$ and 44.60 mg L^{-1} of K_2HPO_4 [34–35]. Glucose is added in the necessary amount to increase the COD value of the prepared synthetic wastewater to the appropriate level. Table 1 presents the characterization of synthetic wastewater.

Table 1 Characteristics of synthetic wastewater

Parameters	Range	Unit
pH	8±0.25	-
COD	40,000±635	mg L^{-1}
Colour	6,386±147	Cu
Turbidity	942 ± 36.38	FTU
NH_3-N	278 ± 49.23	ppm
Total dissolved solid	21.76 ± 3.41	ppt

6) Experimental setup

Using synthetic wastewater, the photocatalytic effectiveness of $CaTiO_3$ was assessed. Three 11 W UV lamps were used as the light source in the photocatalytic reactor. The gap between the UV light source and the top of the wastewater solution in the beaker was 100 mm. Before the photocatalytic analysis, the photocatalyst dosage was mixed with 150 mL of synthetic wastewater. The resulting solution was constantly stirred at 120 rpm for 30 min at a time while it was in the dark using a magnetic stirrer for adsorption-desorption. After that the mixture was put into the photoreactor and the UV light source was turned ON. 5 mL of the solution was removed regularly to calculate the COD. Figure 1 shows the schematic of the photoreactor used in this study.

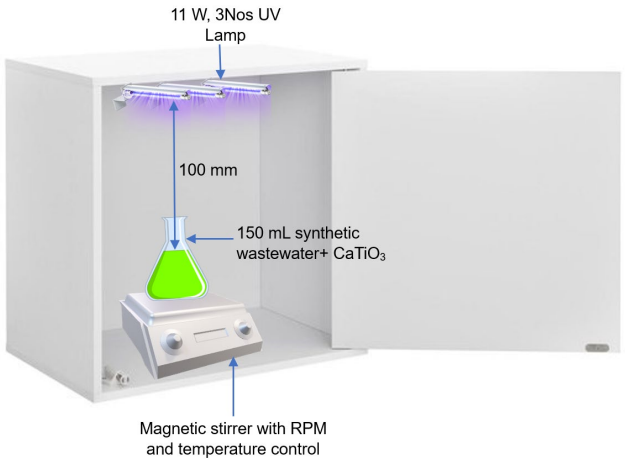

Figure 1 Schematic of photoreactor used in this study.

7) Photocatalytic performance evaluation method

The initial pH of the synthetic wastewater was 8±2.5. The pH was stabilized by using sulfuric acid and decreased to 6. After that, the necessary amount of $CaTiO_3$ dose is added to 150 mL of the pH-stabilized wastewater. The solution was magnetically stirred for 30 min in the dark to ascertain adsorption-desorption equilibrium. After that, the solution was continually stirred while the UV lights were ON. The COD measurement procedure is as per Indian standard IS: 3025 (Part 58) - Reaffirmed 2006. The following is the methodology used to measure COD from wastewater:

(a) Three COD vials with stoppers should be taken. To each of the two COD vials, add 2.5 mL of the sample. The last COD vial is for the blank; add distilled water to it.

(b) Fill each of the three COD vials with 1.5 mL of the potassium dichromate reagent-digestion solution. Continue in the same way to add 3.5 mL of the sulphuric acid reagent-catalyst solution.

(c) Now switch on the COD Digester and set the temperature at 150 °C and time at 2 h. Place the COD vials into a block digester and heat for two hours.

(d) Fill the burette with the ferrous ammonium sulphate solution, adjust it to zero, and fix the burette to the stand. Transfer the contents of the blank vial to the conical flask.

(e) Now add a few drops of ferroin indicator. The solution becomes bluish-green in colour. Titrate it with the ferrous ammonium sulphate taken in the burette. The endpoint of the titration is the appearance of the reddish brown colour.

(f) The proportion of COD eliminated was calculated using the following formula:

$$\% \text{ COD removal} = \frac{Co-C}{Co} \times 100$$

where C represents the measured COD after titration of the sample and C_o represents the measured COD before titration of the sample.

Results and discussion

1) Characterization of $CaTiO_3$

TGA and DTA investigations were carried out to ascertain the optimal CT for synthesis. Using a DTA and TGA curve, Figure 2(a) illustrates the temperature evolution of the pre-calcined $CaTiO_3$ nanoparticle (NP). According to Figure 2(a), these peaks correspond to mass losses of 74.21%. The sample's weight loss was negligible at temperatures over 620 °C. Based on the obtained results, it is noted that the primary physico-chemical processes that result in the acquisition of the target oxide take place below 620 °C. Over this temperature, the sample's weight stays nearly constant, indicating that the processes have finished and the $CaTiO_3$ crystalline phase has formed. This led to defining 600 °C temperature to thermally treat the pre-calcinate and obtain the $CaTiO_3$ nanoparticles.

The crystalline nature and signal-phase ortho-rhombic structure of $CaTiO_3$, as illustrated in Figure 2(b), is confirmed by the strong peaks of the XRD pattern at 600 °C, and this pattern matches precisely the ICDD (International Code of Diffraction Data) card No.: 98-018-5448 and 98-018-5446. The lattice parameters have values of a = 5.632, b = 5.375, and c = 7.356 all in Å and $\alpha = \beta = \gamma = 90°$ which shows $CaTiO_3$ nanoparticles were orthorhombic ($a \neq b \neq c$; $\alpha = \beta = \gamma = 90°$) signal-phase structure. The nanoparticles with a size smaller than 35.97 nm are visible in Figure 2(c) and Figure 2(d). The EDX spectra (Figure 2(e)), show distinct peaks for the elements O, Ti, and Ca, and also, the absence of any secondary elements demonstrates the purity of synthesized nanoparticle. The size of irregularly shaped nanoparticles varies from 12.52 to 47.62 nm as shown in TEM images (Figure 2(f) and Figure 2(g)).

Figure 2(h) shows the band gap calculation of the $CaTiO_3$ nanoparticles. The band gap of the $CaTiO_3$ nanoparticle was 3.57 eV. The band gap was calculated using Tauc's equation, $K(h\nu - Eg) = (\alpha h\nu)^n$, where the Plank constant, frequency of light, band gap, constant, and absorption coefficient are represented by the variables h, ν, Eg, K, and α, respectively. The direct band gap is indicated by n = 2 for $CaTiO_3$. To compute the band gap energy, the linear part of $(\alpha h\nu)^2$ vs hν was extrapolated to the point α equal to zero.

2) Characterization of doped-$CaTiO_3$

In Figure 3(a), the impact of doping on the XRD pattern is illustrated. A secondary phase formation was seen in the XRD patterns of doped $CaTiO_3$, specifically in the cases of Fe and Cu-doped $CaTiO_3$. However, V-doped $CaTiO_3$ does not exhibit any secondary phase formation. Figures 3(b), 3(c) and 3(d) display the doped $CaTiO_3$ FESEM images.

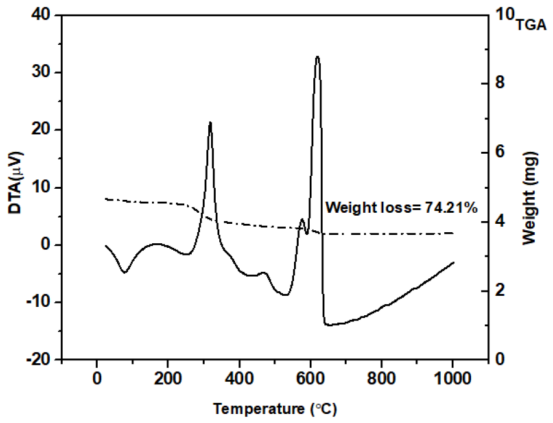

(a) TGA and DTA analysis.

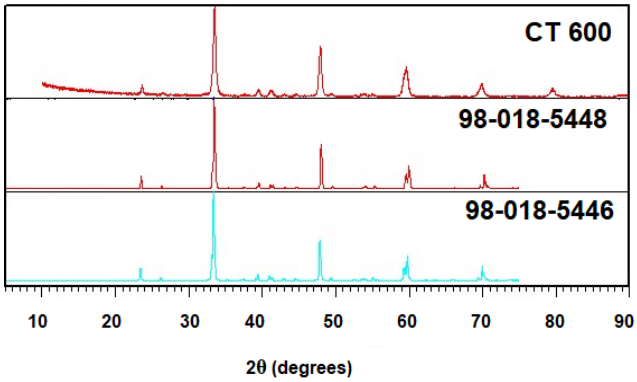

(b) XRD pattern.

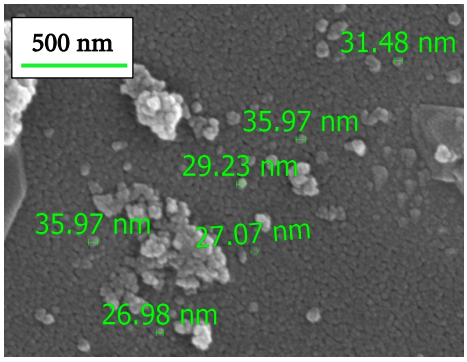

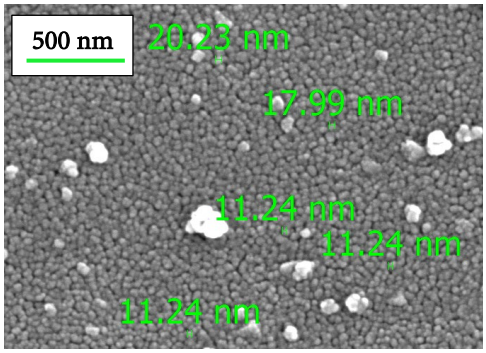

(c) FESEM image.

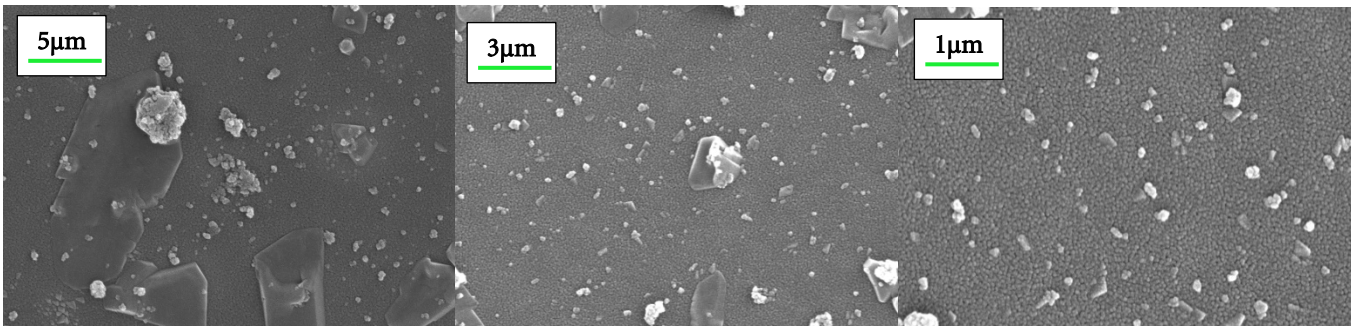

(d) FESEM image.

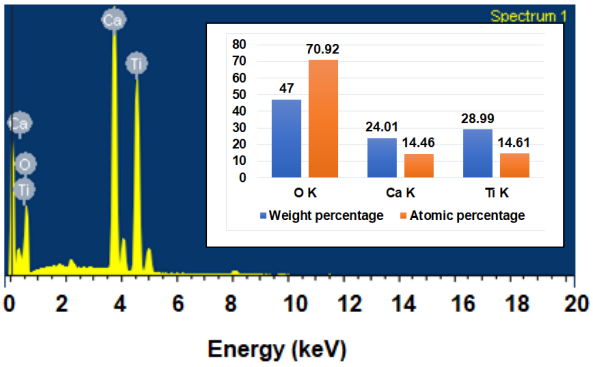

(e) EDX spectrum.

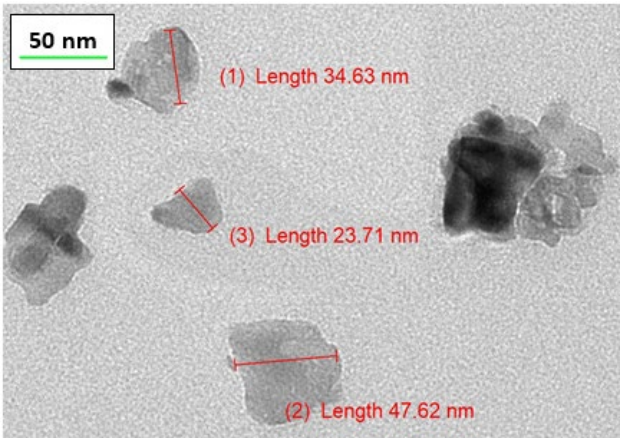

(f) TEM images.

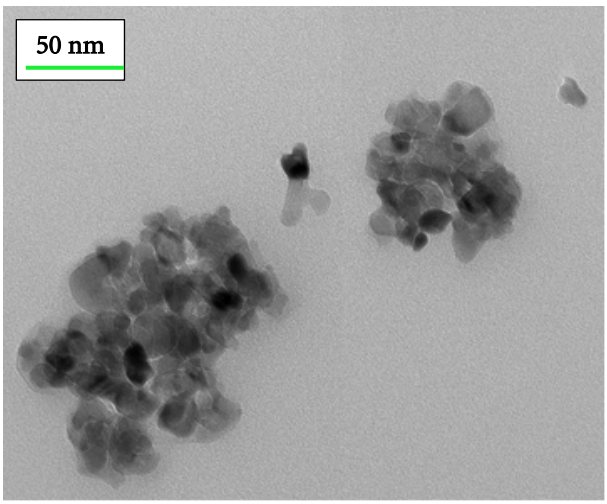

(g) TEM images.

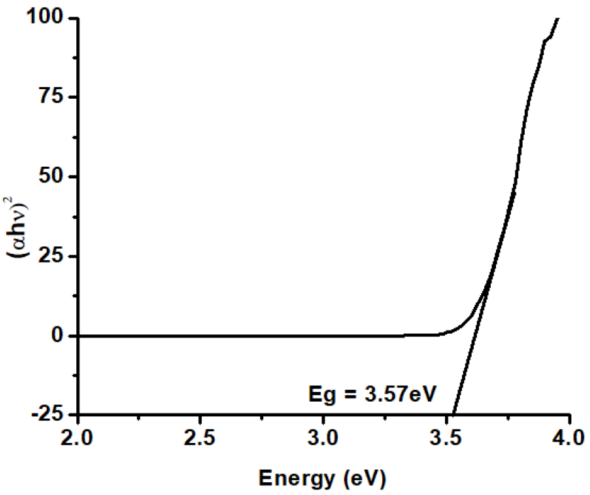

(h) Band gap of $CaTiO_3$.

Figure 2 Characterization of $CaTiO_3$.

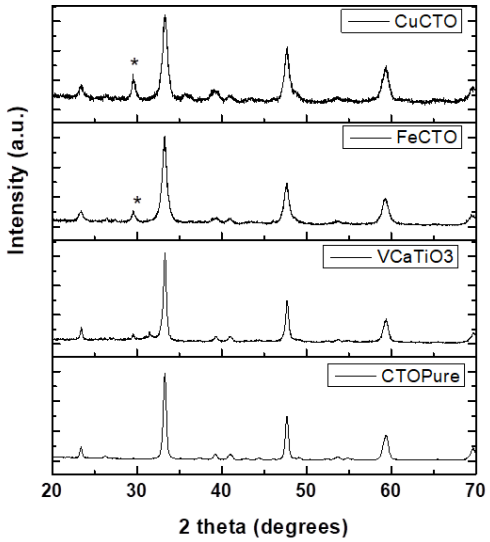

(a) XRD pattern of doped $CaTiO_3$.

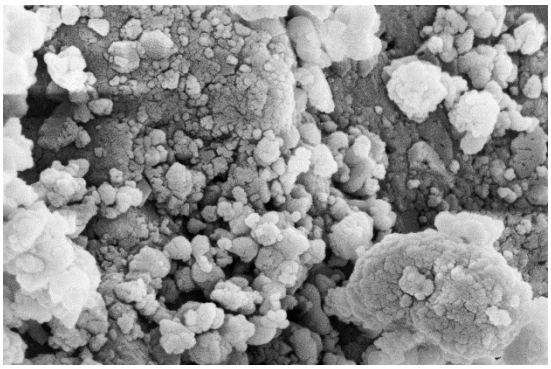

(b) FESEM image of Fe-doped $CaTiO_3$, scale 100 nm.

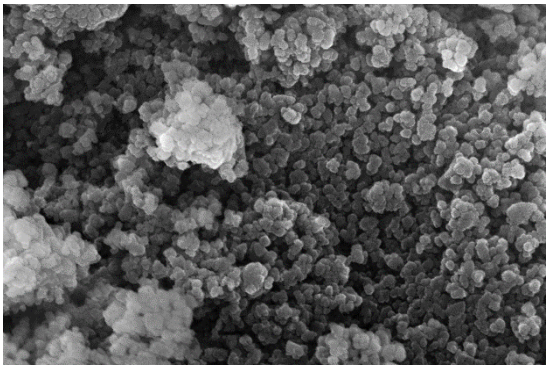

(c) FESEM image of V-doped $CaTiO_3$, scale 100 nm.

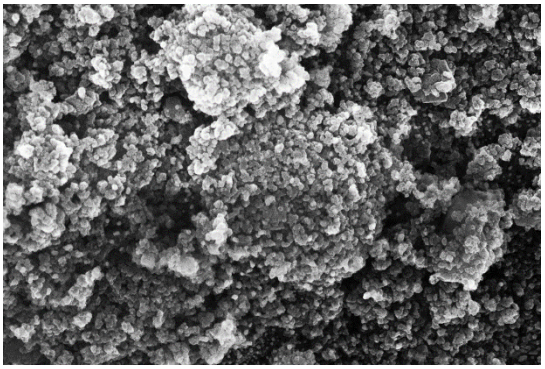

(d) FESEM image of Cu-doped $CaTiO_3$, scale 100 nm.

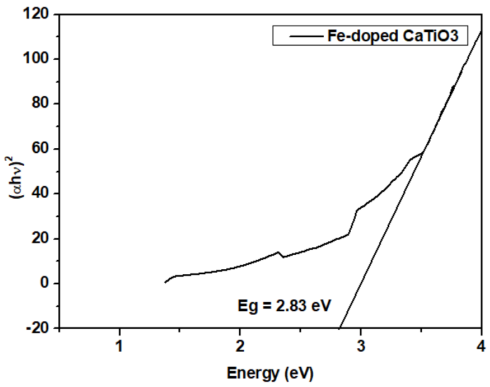

(e) Band gap of Fe-doped $CaTiO_3$.

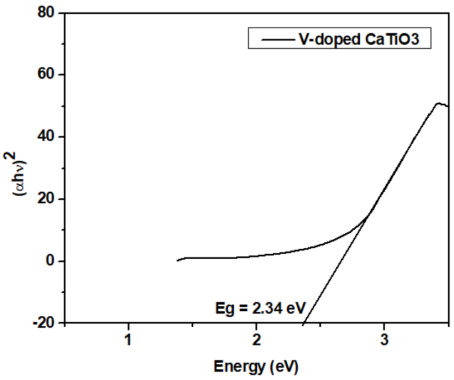

(f) Band gap of V-doped $CaTiO_3$.

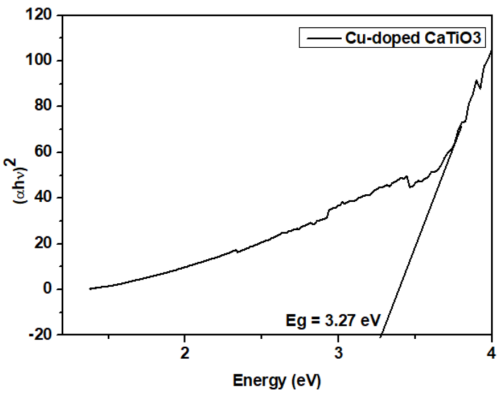

(g) Band gap of Cu-doped $CaTiO_3$.

Figure 3 Characterization of doped $CaTiO_3$.

The effect of doping on the band gap (BG) of $CaTiO_3$ using Fe, V, and Cu as dopants is shown in Figures 3(e), 3(f), and 3(g). In the ultraviolet portion of the solar spectrum, $CaTiO_3$, an n-type semiconductor, exhibits optical absorption. There is a BG of 3.57 eV between the $CaTiO_3$ empty CB and its e^--rich VB at CT of 600 °C. Doping foreign materials into UV-responsive photocatalysts is an approach frequently utilized to produce efficient and visible light-responsive photocatalysts [12]. At one of the host material crystal lattice points, a metal or non-metal element is replaced. The most significant effect of dopants is the improvement of $CaTiO_3$ electronic structure, which makes it less susceptible to UV light and increases its ability to absorb visible light. This makes $CaTiO_3$ suitable for the widespread use of photocatalytic treatment [18]. The BG of $CaTiO_3$ can be lowered by introducing localized energy levels within the BG, raising the VB minimum, reducing the CB minimum, or all three depending on the type of dopant used. Doping is primarily used to slow down quick charge recombination and improve visible light absorption [12, 18, 36, 37]. In addition to producing e^--h^+ pairs and photocatalytic activity at a particular wavelength, the BG is also responsible for lowering the rate of recombination. The h^+ and e^- pairs are formed when photons have an energy equal to or greater than the photocatalyst BG. The ultimate objective is to decrease the BG so that visible light can excite the photocatalyst [38]. UV light has a wavelength range of 100–400 nm (UVC, 100–280 nm, UVB, 280–315 nm, and UVA, 315–400 nm), whereas visible light has a wavelength range of 400–750 nm. The range of photon energy necessary for the creation of e^--h^+ pairs is 3.10 to 3.94 eV for UVA, 3.94 to 4.43 eV for UVB, 4.43 to 12.4 eV for UVC, and 1.5 to 3.09 eV for visible light when $E(eV) = h\nu = 1240/\lambda(nm)$ [36]. Since UV light is the primary trigger for most photocatalysts, a constant source of light is needed to maintain the reaction, which raises maintenance costs and necessitates ongoing system upkeep in the event of large-scale adoption. For the doped photocatalyst that functions under visible light, sunlight is sufficient to initiate the photocatalytic mechanism [39].

Doping with transition metals (Fe and Cu): Another method for modifying photocatalysts that are driven by visible light is transition metal-ion doping. It is possible to prevent the recombination of e^--h^+ pairs and prolong the life of the carriers by creating lattice defects or modifying the crystallinity of a material by adding transition metal ions [12, 18]. Because certain metal ions can produce a wide range of new energy

levels below CB due to their partially filled d-orbitals, doping with these ions can also extend the light absorption zone. This can cause a redshift in the BG and increase the responsiveness to visible light. Photo-electrochemical characteristics of semiconductors are significantly influenced by the shifts in valence states and 3d orbits of transition metals [18]. Due to its distinctive half-filled electronic configuration, doping with Fe is known to provide higher photocatalytic performance as compared to doping with other metals having closed-shell electronic configurations. Between the VB and CB, impurity energy levels formed as a result of the Fe doping and lower the BG [18]. At a calcination temperature of 600 °C, Fe-doped $CaTiO_3$ was synthesized using the sol-gel method. The Fe substitution at the Ti-site in the $CaTi_{1-x}Fe_xO_3$ lattice was shown to significantly reduce the bandgap of $CaTiO_3$ from 3.57 to 2.83 eV and significantly shift the absorption towards the visible range.

At a calcination temperature of 600 °C, Cu^{2+} doped $CaTiO_3$ was synthesized using the sol-gel method. The shift from the donor levels generated by Cu^{2+} 3d orbit to the CB of Cu^{2+}-doped $CaTiO_3$ resulted in a reduction in the band gap of $CaTiO_3$ from 3.57 eV to 3.27 eV.

Doping with rare earth metals (V): Using the sol-gel process, V-doped $CaTiO_3$ is synthesized at a calcination temperature of 600 °C, where V in the titanium site leads to the formation of an energy band directly below the CB, lowering the BG from 3.57 eV to 2.34 eV. The 2p states of O and 3d states of V combine to form this band [24]. The energy band directly below the CB leads to easy migration of e^- and h^+, effectively separating e^- from h^+ to prevent recombination and shifting photocatalytic activity from UV to visible or solar light [18, 24, 37].

The impact of doping on photocatalytic performance and photocatalyst BG on undoped TiO_2, metal-doped TiO_2, and non-metal-doped TiO_2 is shown in Figure 4. As shown in Figure 4, the BG for doped TiO_2 using metal or non-metal is lower than for undoped TiO_2. This means that an e- would require less energy to be excited from the VB to the CB. Doping lowers the energy and wavelength required to absorb light, causing it to shift toward visible wavelengths and enhancing photocatalytic activity [41]. Doping improves BG narrowing [12], impurity energy level introduction [42], and oxygen vacancies [43]. Doping a photocatalyst with a metallic, non-metallic, or sometimes semiconductor has been done to minimize the recombination of e^- and h^+ and to increase the photocatalyst performance under visible light [12, 18]. Doping also reduces the BG difference between the CB and the VB [44].

In this study, the effect of doping on $CaTiO_3$ using V, Cu, and Fe as dopants is shown in Table 2. It has been demonstrated that the BG of $CaTiO_3$ reduced from 3.57 to 2.34 eV after doping, making it possible to treat wastewater photo-catalytically under solar radiation rather than under UV light to expand its large-scale industrial applications.

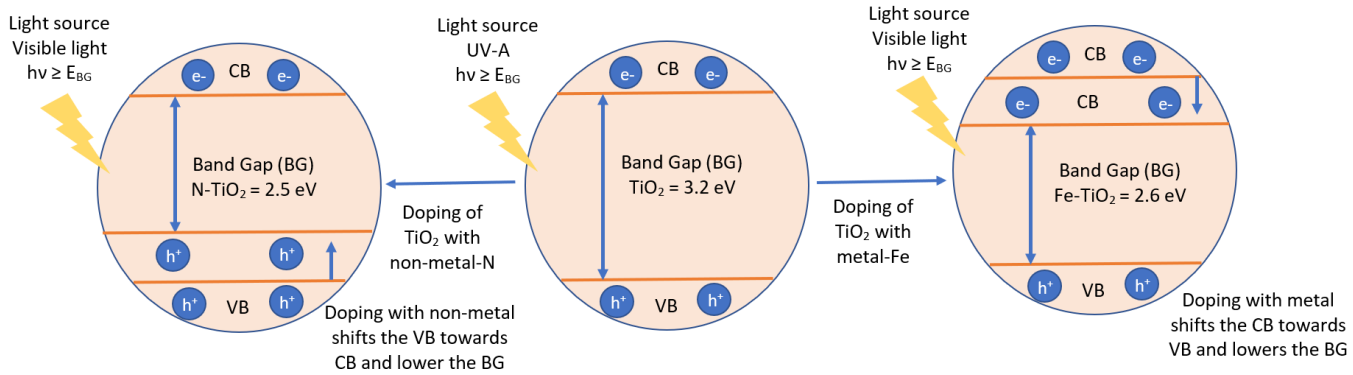

Figure 4 Effect of doping on BG [40].

Table 2 Effect of doping on BG of $CaTiO_3$

Photocatalyst	Band gap	Photocatalytic activity	XRD Pattern
$CaTiO_3$	3.57 eV	UV-light	Matched with ICCD card No. 98-018-5448 and 98-018-5446
Cu-doped $CaTiO_3$	3.27 eV	UV-light	Secondary phase observed
Fe-doped $CaTiO_3$	2.83 eV	Sunlight	Secondary phase observed
V-doped $CaTiO_3$	2.34 eV	Sunlight	No secondary phase observed

3) Effect of operating parameters

3.1) Light intensity

In photocatalytic reactions, the light of different wavelengths serves as the energy source. The higher energy will be coupled with a shorter wavelength. Because of this, contaminants will be degraded more quickly due to a faster response rate. Figure 5(a) shows the photocatalytic mechanism of $CaTiO_3$. The primary phases that occurred when the light was irradiated to photocatalysis are as follows [1, 18, 36, 37]:

1. *Generation of electron (e^-) – hole (h^+) pair*

$$\text{Band gap (BG)} \leq h\nu + CaTiO_3 \text{ photocatalyst} \rightarrow h^+_{\text{Valence band (VB) of } CaTiO_3} + e^-_{\text{Conduction band (CB) of } CaTiO_3}$$

2. *Photooxidation*

$$h^+_{\text{VB of } CaTiO_3} + H_2O \rightarrow H^+ + OH$$

3. *Photoreduction*

$$e^-_{\text{CB of } CaTiO_3} + O_2 \rightarrow O_2^-$$

$$O_2^- + H_2O \rightarrow HO_2$$

$$e^-_{\text{CB of } CaTiO_3} + H_2O_2 \rightarrow OH$$

4. *Contaminant degradation*

$$\text{Contaminant} + \text{Oxidizing Species} \rightarrow \text{Byproduct/Simpler compound} + H_2O + CO_2$$

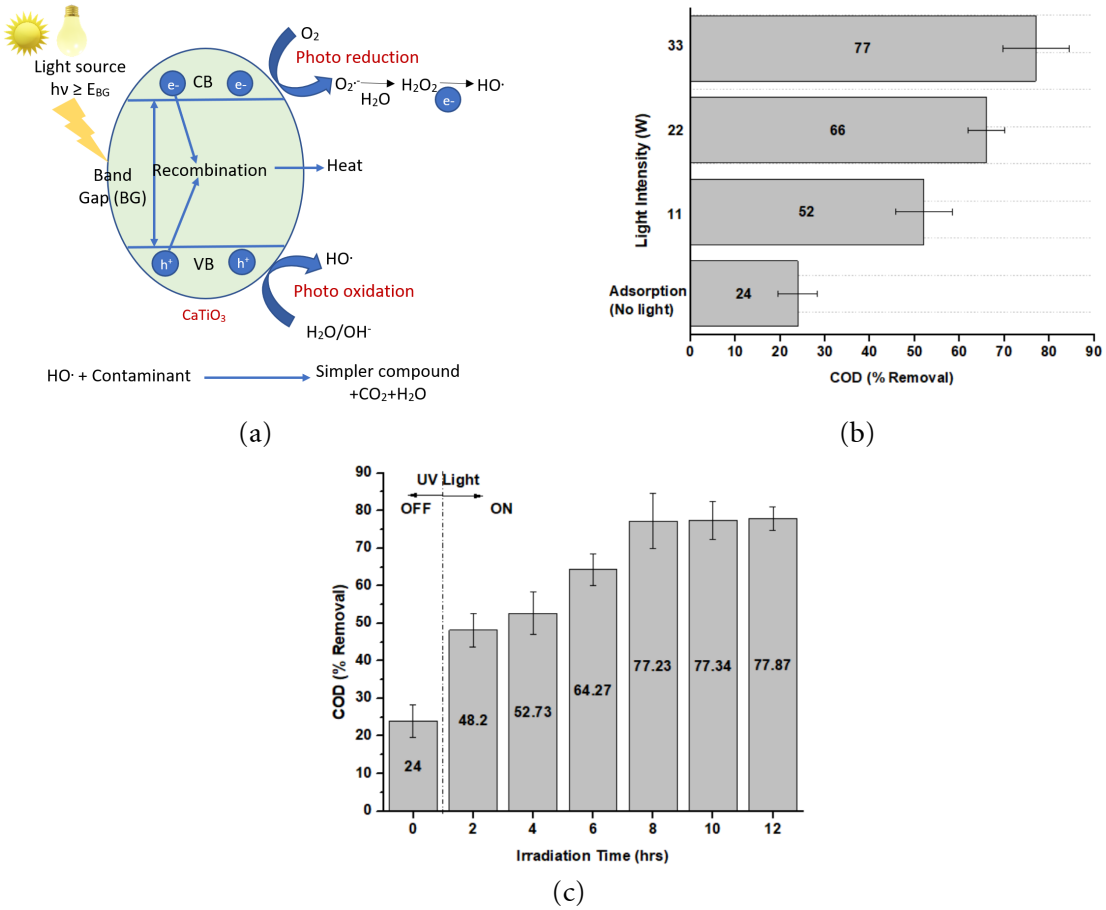

Figure 5 Photocatalytic performance of $CaTiO_3$ including (a) photocatalytic mechanism, (b) effect of light intensity and (c) effect of irradiation time.

$CaTiO_3$ photocatalytic treatment effectiveness as a function of the intensity of light is shown in Figure 5(b). Adsorption accounted for 24% of the COD removal in the absence of UV light. At 11, 22, and 33 W, the percentage of COD removed after 8 h of UV light irradiation was 52%, 66%, and 77% respectively. The efficiency of photocatalysis increases with light intensity as more HO• radicals and super-oxide ions form resulting in more degradation of contaminants and it reaches its maximum at 33W. Further improvement in light intensity shows no significant improvement in removal efficiency as most of the active sites present on the catalyst surface may consumed during the course of the photocatalytic reaction. Similar observations were reported in [45-48]. Therefore, 33 W is considered the optimum value for the photocatalytic treatment.

3.2) Irradiance time

Photocatalysis efficiency increases with longer irradiation times. The higher generation of e^- - h^+ pairs and the interaction of the contaminant with the photocatalyst surface are responsible for the enhancement of the photocatalyst's capacity to degrade contaminants. However, after 8 h of irradiation, the photoactive sites in the $CaTiO_3$ are consumed during the photocatalytic degradation of contaminants and as a result, the percentage of COD removal starts to saturate and becomes approximately constant, as shown in Figure 5 (c). Similar observations were reported in the previous studies [49-50].

3.3) pH

Starting pH is one of the most important elements impacting the photocatalytic degradation of wastewater because it affects the adsorption of contaminants at the surface of the catalyst, which is influenced by the charge on the catalyst surface and aggregate size [50]. Particularly in adsorption tests, it significantly affects the charge on the material surface in an aqueous solution. It is necessary to alter the charge on the material surface and determine the ideal pH levels for adsorption if the material's charge is the same as the adsorbate and prevents adsorption. It is therefore necessary to identify the pH at which the surface charge of adsorbent materials in an aqueous medium is zero, or pH_{zpc}, to determine optimal operating parameters [36, 51–52].

Figure 6 displays the $CaTiO_3$ nanoparticle pH_{zpc}. pH_{zpc} is computed by the pH drift method [53]. By altering the pH of a 20 mL 0.01 mol L^{-1} NaCl solution to a value between 2 and 10, pH_{pzc} was determined. After adding 0.010 g of $CaTiO_3$, the mixture was stirred for 10 h before the final pH was determined. The point where the difference between initial and final pH is zero is known as the pH_{pzc}.

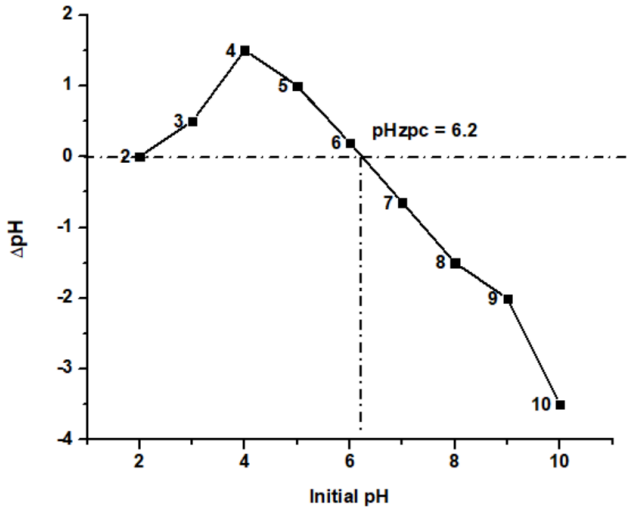

Figure 6 pH_{zpc} using the pH drift method.

In an aqueous solution with a pH higher than pH_{zpc}, the photocatalyst surface was negatively charged, which aided in the adsorption of cations and, consequently, the oxidation of cationic electron acceptors and donors. The adsorbent surface was positively charged when the pH of the adsorbent was lower than pHzpc, which encourages the adsorption of anions [37, 51]. Consequently, more protons are donated by acidic water than by hydroxide groups [54].

Photocatalytic performance is suboptimal at alkaline or acidic pH, but it is remarkably efficient at neutral pH [48]. TiO_2 can produce negative or positive charges on its surface due to an amphoteric characteristic [50], hence changes in pH can affect the adsorption of contaminants on its surfaces. As a result, the pH must be chosen carefully to obtain optimal degradation efficiency. The separation of the photogenerated e^--h^+ pairs and the adsorption-desorption processes in the photocatalyst surface are influenced by the pH of the solution, which also affects the charge carriers generated on the photocatalyst surface [54–55]. A variety of factors influence the optimal pH, including the type of contaminants and the pH at which photocatalysts have zero charges (pH_{zpc}). Because leachate contains a variety of contaminants, having both positive and negative charge contaminants, and photocatalysts have a neutral surface charge at pH_{zpc}, all of the contaminants may come into contact with the photocatalyst's surface and exhibit maximum photocatalytic efficiency as a result of mixing the two materials [56]. The acidic range was found to contain the ideal pH [57–58]. Nevertheless, the findings of the experiments indicated that the specific surface area of the nanoparticles is decreased and they quickly agglomerate at pH values lower than 4. According

to the results of the experiment conducted by Amakiri et al. [36], the size and quantity of aggregated TiO_2 particles increased when the pH of the leachate was lowered from 5.4 to 3.9. The effect of pH on $CaTiO_3$ photocatalytic performance is demonstrated in Figure 7(a). When applied to wastewater treatment, $CaTiO_3$ exhibits its highest photocatalytic efficacy in the acidic range, or pH value of 6. The pH_{zpc} value of $CaTiO_3$ nanoparticles was approximately 6.2. Research indicates [56, 59] that at a pH near pH_{zpc}, the optimum efficacy of photocatalytic removal and the most adsorption of contaminants occur. At pH_{zpc}, the repellent force between pollutants and nanoparticles is minimal due to the neutral surface charge of the nanoparticles at that particular pH. By mixing the $CaTiO_3$ nanoparticles in wastewater, all contaminants can therefore come into touch with the surface of the nanoparticles, and at pH 6, which is nearly equal to pH_{zpc}, the percentage of COD removal reached its maximum. Due to repulsion between the charged impurity and the surface of the $CaTiO_3$ nanoparticle, the percentage of COD removal decreases at pH values other than 6, indicating the presence of an electrostatic component.

3.4) Catalyst dose

As $CaTiO_3$ doses increased from 0.1 to 0.5 g per 150 mL of wastewater, the percentage of COD removed increased as well. However, beyond that point, the percentage of COD removed begins to decrease because light cannot get through, making most of the catalyst surfaces inactive, as can be observed in Figure 7(b). So, the optimum value of the catalyst dose for wastewater treatment is 3.33 g L^{-1} (0.5 g per 150 mL). A similar trend is reported in previous studies [50, 60]. The percentage of COD removed increases from 28% to 72% when the catalyst dose rises from 125 to 1000 mg L^{-1}, after which it stays constant up to a dosage of 2000 mg L^{-1}. The simple link between photocatalytic efficiency and catalyst dose is that the number of radicals needed for degradation and, consequently, the reaction rate, both increase with catalyst dose [12]. Raising the catalyst dose will have little effect, though, after the reaction reaches its maximum efficiency because light cannot travel through the turbid solution and the bulk of the catalyst surfaces become inactive [36, 49]. Moreover, the quantity of active sites on the photocatalyst surface that are available for photocatalytic degradation is decreasing due to the aggregation of nanoparticles at high concentrations [37].

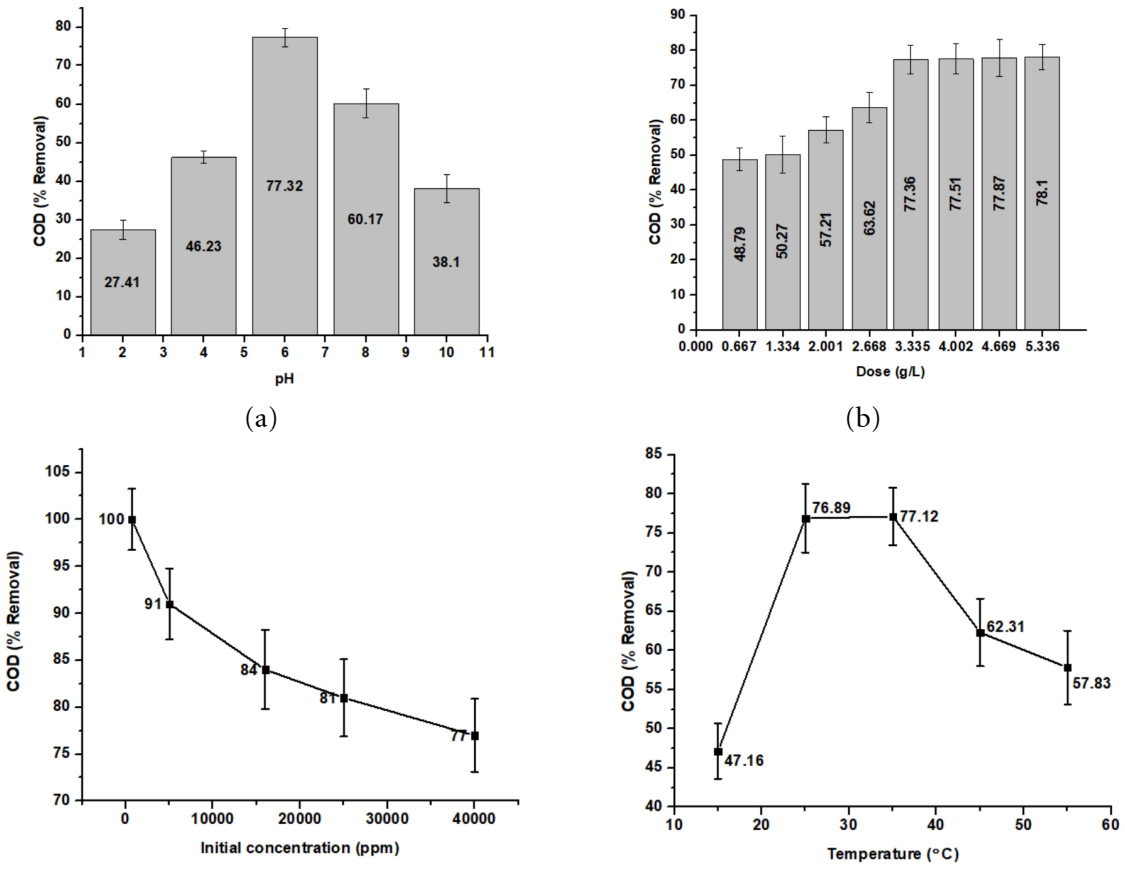

Figure 7 Effects of parameters on the photocatalytic performance of $CaTiO_3$ including (a) pH, (b) catalyst dose, (c) initial COD concentration and (d) reaction temperature.

3.5) Initial COD concentration

The present investigation involved the photocatalytic treatment of synthetic wastewater with varying COD concentrations, varying from 700 to 40000 mg L^{-1}, utilizing 3.33 g L^{-1} of $CaTiO_3$. A pH of 6 and a 33 W UV light with an 8 h irradiation time were the other operational conditions. According to Figure 7(c), as the starting COD concentration increased the efficiency of the photocatalytic process reduced from 100% to 77% while all other operational parameters remained the same. As the initial concentration of contaminants increases, the amount of photocatalyst surface required for degradation grows as well. Because the irradiation time and catalyst dose were both constant, the number of oxidizing radicals generated on the surface of the photocatalyst was also constant. Due to this, as the concentration of contaminants rises, the number of free radicals targeting the contaminant decreases [12, 55]. The length of the photon path or the number of photons, as they approach the photocatalytic surface, was also reduced when the initial concentration of an organic compound increased [36–37]. Consequently, the excitation of an e^- from the VB to the CB is reduced. When all other operating parameters were held constant, the removal rates of direct black 38, Congo red, and methyl orange fell considerably from 99.65%, 99.14%, and 99.53% to 40.64%, 48.03%, and 56.61%, respectively, when the starting dye concentration was increased. Furthermore, photon adsorption by the photocatalyst was reduced as a result of photons being stopped before they could reach the surface of the catalyst. Consequently, the removal rate dropped at high initial dye concentrations [61]. When the initial concentration of contaminants was increased beyond a certain threshold, photocatalytic degradation of contaminants was reduced. This occurred as a result of a significant portion of light being absorbed by the contaminant during adsorption, instead of the photocatalyst, when the surface of the catalyst was completely covered by contaminants. Because contaminant molecules occupy active sites that are inaccessible for photocatalysis, photons reaching the surface of the catalyst, as well as the number of HO• radicals and h^+ created, is reduced [12].

3.6) Reaction temperature

The reaction temperature is adjusted from 10 to 60 °C to determine the impact of this temperature variation on the photocatalytic performance of $CaTiO_3$ under 33 W UV light, 3.33 g L^{-1}, and 8 h irradiation time. Remi 2 L magnetic stirrer with hot plate 2MLH has a heating plate that allows the reaction temperature to be adjusted or controlled. Before the photocatalytic process begins, the necessary temperature is set. A thermometer is used to continuously monitor the reaction temperature. The temperature knob on the stirrer is used to regulate temperature if it rises above the necessary reaction temperature. Because fewer free e^--h^+ pairs were produced at temperatures below 25°C, the percentage of COD eliminated decreased. Additionally, the e^--h^+ pair recombination was facilitated by temperatures above 35°C, resulting in a decrease in the quantity of free e^--h^+ pairs needed for photocatalytic action. The photocatalytic activity of $CaTiO_3$ is maximum at room temperature (25 to 35°C) as shown in Figure 7(d). The majority of photocatalytic reactions occur at room temperature. The reaction temperature rises as a result of e^--h^+ pair recombination and energy released during contaminant breakdown. The rate of photocatalytic breakdown rises with reaction temperature [12]. After a while, the rate of photodegradation begins to drop. Because exothermic contaminant adsorption limits photocatalytic degradation effectiveness at higher temperatures [37]. High temperatures promote recombination by lowering the number of free e^--h^+ pairs needed for the photocatalytic breakdown of contaminants [12, 5, 62].

3.7) Calcination temperature (CT)

The CT has a considerable impact on the optical characteristics, particle size, and surface area of the synthesized nanoparticles. Additionally, high-CT is widely employed to transform amorphous matter into crystal structure during the synthesis of nanoparticles. These CTs frequently led to the agglomeration of nanoparticles, which reduces surface area and lowers the effectiveness of photocatalytic degradation [37, 62–64]. A smaller particle size increases the surface area of the nanoparticles, which eventually improves their interaction with contaminants and optimizes their dispersion in a solution. As a result, their photocatalytic performance increases [65]. Therefore, increasing photocatalytic activities requires a combination of the presence of active sites, particle size, and surface area. In this case, high crystallinity small particle sizes are essential because of their greater specific surface areas, which promote increased photocatalytic activity. The crystalline size of NP increased with CT because of the tendency for interfacial surface energy decrease. Additionally, higher CT produced more diffusion atoms. More nuclei with pores separating the grain boundary were created as a result of the increase in atom diffusion. As the CT increased gradually, the crystalline size increased and the grain boundary disappeared [66–67]. To create nanoparticles with high crystallinity, large CT synthesis is occasionally necessary, but it also generates larger

particles [23, 41–42]. To find out how CT affects photocatalytic performance, the $CaTiO_3$ nanoparticles are synthesized in this study at 400, 500, 600, 700, and 800 °C CT using a sol-gel method as shown in Figure 8 (a). $CaTiO_3$ phase formation began above 600 °C and beyond. The band gap at various calcination temperatures is displayed in Figure 8(b), and FESEM images at 800, 700, and 600 °C CT are displayed in Figures 8(c), 8(d), and 8(e). However, nanoparticles synthesized at CT of 600 °C show the best photocatalytic performance as shown in Table 3 which follows similar findings reported in the literature [37, 63–65].

Breakdown of organic compounds → CO_2 +H_2O +Heat

Recombination of e^--h^+ pair $\xrightarrow{\text{Increase in temperature}}$ Radiation less decay

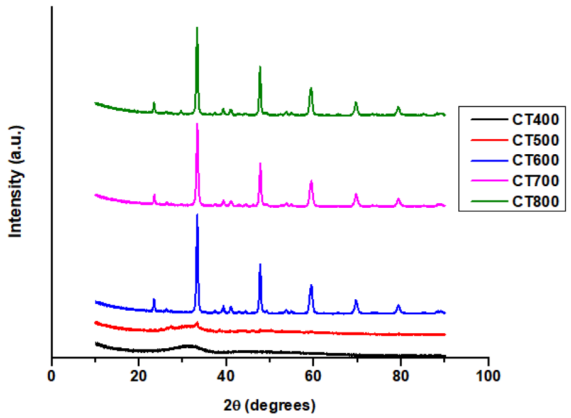

(a) XRD pattern of $CaTiO_3$ at different CT.

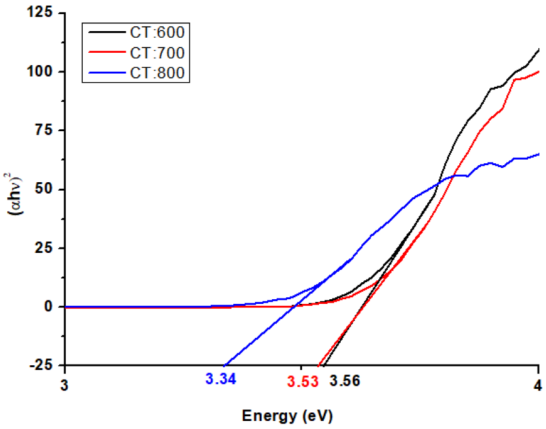

(b) Band gap of $CaTiO_3$ at different CT.

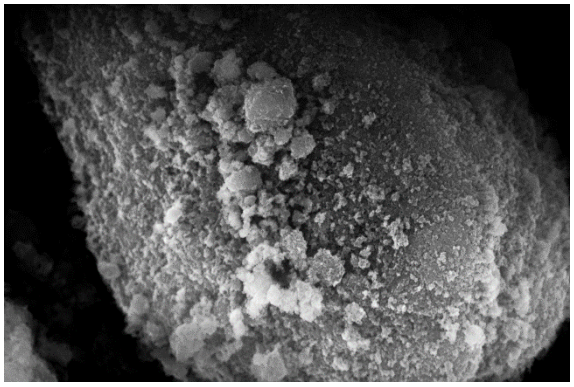

(c) FESEM image of $CaTiO_3$ at 800 °C CT and scale:1µm.

(d) FESEM image of $CaTiO_3$ at 700 °C CT and scale:1µm.

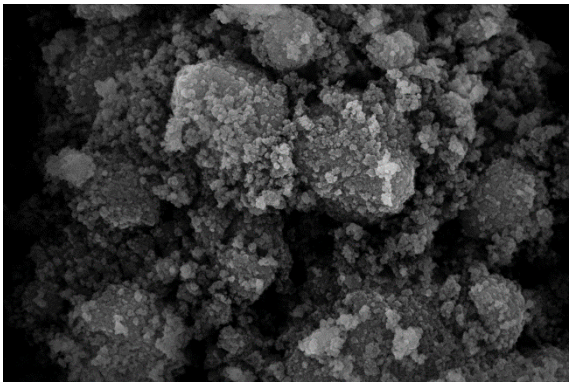

(e) FESEM image of $CaTiO_3$ at 600 °C CT and scale:1µm.

Figure 8 Effect of CT on $CaTiO_3$ nanoparticle.

Table 3 Effect of calcination temperature of $CaTiO_3$

CT (° C)	Band gap (eV)	Particle size (nm)	Surface area ($m^2 g^{-1}$)	% COD removal (Initial COD = 16,000 mg L^{-1})
600	3.56	54.25	98.64	84%
700	3.53	78.01	62.57	78%
800	3.34	95.47	51 .12	72%

3.8) Oxidant

The inclusion of oxidizing agents such as ClO_4^-, $S_2O_8^{2-}$, BrO_3^-, H_2O_2, and O_3 increased the efficacy of photocatalytic breakdown of contaminants substantially [37, 55]. By increasing the amount of unpaired e^-, these oxidants inhibit recombination and generate oxidizing radicals, which may enhance the photocatalytic degradation of contaminants. With the addition of H_2O_2, the concentration of radical anions and radicals increases, leading to an improvement in photocatalytic activities [12]. The process by which radical anions and radicals are produced when H_2O_2 is added can be represented as follows:

$$H_2O_2 + h\nu \rightarrow HO\bullet + HO\bullet$$

$$H_2O_2 + e^- \text{ in CB} \rightarrow HO\bullet + OH^-$$

$$H_2O_2 + O_2^{\bullet -} \rightarrow HO\bullet + OH^- + O_2$$

The addition of H_2O_2 could speed up the reaction by generating more HO• radicals. The production of more HO• radicals enhanced the oxidation process of contaminants present in wastewater. In the present study, the percentage of COD removal from synthetic wastewater having a COD concentration of 40,000 mg L^{-1} improved from 77.12% to 86% with the addition of 0.01M H_2O_2 under optimum conditions of 33 W UV light, 3.33 g L^{-1} of catalyst dose, and irradiation time of 8 h.

3.9) Radical scavengers

The percentage of COD removed from synthetic wastewater decreased from 77.12% (when no scavenger was present) to 67.50% by adding 0.01 mM of HCO_3^- anions and to 60.13% by adding 0.01 mM of Cl^- anions for the initial COD concentration of 40,000 mg L^{-1} under optimum conditions of 33 W UV light, 3.33 g L^{-1} of catalyst dose, and irradiation time of 8 h. Cl^- and HCO_3^- anions negative effects can be linked to their adsorption on the active sites of the $CaTiO_3$ nano-photocatalyst and their scavenging interactions with HO•, superoxide, and/or h^+ radicals. As a result, fewer HO•, superoxide, and/or h^+ radicals are available for the degradation of the contaminant as shown in the equations that follow:

$$HCO_3^- + HO\bullet \rightarrow H_2O + CO_3\bullet^-$$

$$Cl^- + HO\bullet \rightarrow HO^- + Cl\bullet$$

$$Cl^- + h^+ \rightarrow Cl\bullet$$

The effect of oxidant and radical scavenger on the photocatalytic performance of $CaTiO_3$ is shown in Figure 9.

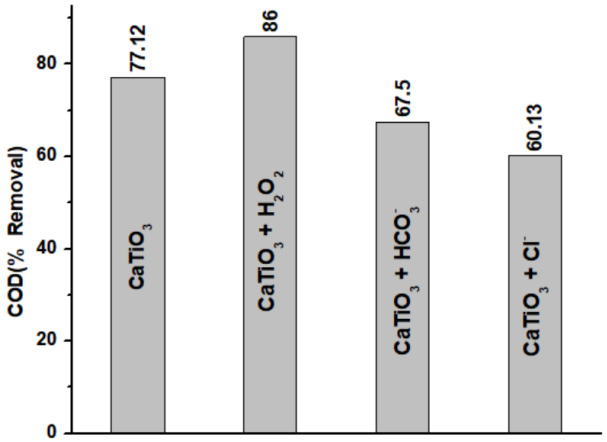

Figure 9 Effect of oxidant and radical scavenger on the photocatalytic performance of $CaTiO_3$.

Table 4 compares the photocatalytic performance of $CaTiO_3$ in this study with previous findings. According to a review of the literature, [19–28, 64–69] investigate the effects of pH, irradiation time, light intensity, catalyst dose, initial concentration of pollutant, calcination temperature, doping, presence of scavengers and oxidant on the photocatalytic performance of $CaTiO_3$. The comparative analysis of how these operational parameters affect $CaTiO_3$ photocatalytic performance is presented in Table 5. The range (R), optimum value (O), and trend (T) of each parameter are shown in Table 5.

Table 4 Comparison of photocatalytic performance of $CaTiO_3$

Photocatalyst	Type of Wastewater	Target pollutant	Operating condition	Removal efficiency	Ref
$CaTiO_3$	Synthetic wastewater	COD	Light source: UV Light intensity: 33 W pH: 6.2 Catalyst dose: 3.33 g L^{-1} Irradiation time: 480 min Initial COD concentration: 700, 16,000, 40,000 mg L^{-1}	100% at 700 mg L^{-1} 84% at 16000 mg L^{-1} 77% at 40,000 mg L^{-1}	This study
$CaTiO_3$ + H_3PO_4	Simulated dye solution	Rhodamine B (RhB)	Light source: UV Light intensity: 15 W Irradiation time: 180 min Catalyst dose: 0.1 g Initial concentration: 3 mg L^{-1}	85%	[15]
$CaTiO_3$	Textile- and tannery wastewater	COD	Light source: UV Light intensity: 125 W pH: 11.2 $CaTiO_3$ dose: 1g L^{-1} Irradiation time: 240 min Initial COD for textile wastewater: 148 mg L^{-1} Initial COD for tannery wastewater: 323 mg L^{-1}	45% for textile 46% for tannery wastewater	[16]
$CaTiO_3$	Simulated wastewater, river and lake surface water	COD Methylene blue (MB)	Light source: UV Light intensity: 30 W pH:5-7 Irradiation time: 120 min $CaTiO_3$ dose: 1g L^{-1} MB concentration: 10 mg L^{-1} Initial COD for river water: 44.218 mg L^{-1} Initial COD for lake water: 65.638 mg L^{-1}	56% for COD of simulated wastewater 64.26 % for river surface water 67.65% for lake surface water 84.13% for MB	[19]
$CaTiO_3$	Dye solution	COD	Light source: UV Catalyst dose: 0.5 g L^{-1} Irradiation time: 120 min Initial concentration: 742 mg L^{-1}	93.5%	[29]
$CaTiO_3$	Dye solution	MB	Light source: UV Light intensity: 11W Catalyst Dose: 0.5 g L^{-1} Irradiation time: 330 min	97%	[30]
MoS_2+$CaTiO_3$	Dye solution	RhB	Light source: Visible Light intensity: 15 W Catalyst Dose: 0.01 g Irradiation time: 180 min IC: 1 mg L^{-1}	19% at $CaTiO_3$ 97% at MoS_2+$CaTiO_3$	[31]
$CaTiO_3$	Simulated dye solution	Methyl orange (MO)	Light intensity: 500 W Simulated solar light Catalyst dose: 15 mg MO concentration: 50 mL of 10 mg L^{-1} Irradiation time: 40 min	99.03% by rod-like $CaTiO_3$ 98.15% by grainy $CaTiO_3$	[32]

Table 5(a) Comparative study on the effect of operating parameters on the photocatalytic performance of $CaTiO_3$

Parameter		Reference					
		19	20	21	22	23	24
Photocatalyst		$CaTiO_3$	$CaTiO_3$	$CaTiO_3$	Eu + $CaTiO_3$	B-SiO_2 + $CaTiO_3$	V + $CaTiO_3$
Effect of pH	R	0 to 9	-	3 to 8	-	-	-
	O	4	-	7	-	-	-
	T	Heavy metal removal rate (RR) increases up to the optimum value after that no significant change is observed	-	-	-	-	-
Effect of irradiation time (h)	R	0 to 2	-	0 to 8	0 to 100 min	-	0 to 2
	O	20 min	-	8	100 min	-	-
	T	Heavy metal RR increases up to the optimum value after that no significant change is observed	-	RR increases as irradiation time increases	RR increases as irradiation time increases	-	RR increases as irradiation time increases
Effect of light intensity/illumination wavelength	R	-	200 to 500 nm	-	-	-	-
	O	-	300 nm	-	-	-	-
	T	-	MB RR increases up to the optimum value and then starts decreasing	-	-	-	-
Effect of catalyst dose	R	-	1 to 10 g L^{-1}	50 to 200 mg	10 to 50 mg L^{-1}	0.01 to 0.08 g	-
	O	-	8 g L^{-1}	100 mg	-	0.025 g	-
	T	-	MB RR increases up to the optimum value after that it starts decreasing	RR increases up to the optimum value after that no significant improvement is observed	MO RR 92% at 10 mg L^{-1} 95% at 50 mg L^{-1}	RR increases up to the optimum value after that no significant improvement is observed	-
Effect of initial concentration (IC) of pollutant	R	-	2 to 10 mg L^{-1}	5 to 20 mg L^{-1}	-	25 to 100 mg L^{-1}	-
	O	-	-	-	-	-	-
	T	100% at 60 mg L^{-1} ofNi 90.9% at 68.22 mg L^{-1} of Ni 100% at 240 mg L^{-1} ofPb 93% at 299.15 mg L^{-1} of Pb	RR decreases as IC increase	RR decreases as IC increase	-	94% at 25 mg L^{-1} 91% at 50 mg L^{-1} 69% at 100 mg L^{-1}	-

Table 5(a) Comparative study on the effect of operating parameters on the photocatalytic performance of $CaTiO_3$

Parameter		Reference					
		19	**20**	**21**	**22**	**23**	**24**
Effect of calcination temperature (CT) (°C)	R	750, 900 and 1050	-	-	500, 700 and 900	-	-
	O	900	-	-	900	-	-
	T	-	-	-	MO removal rate 52% at 500 °C 78% at 700 °C 93% at 900 °C	-	-
Effect of doping	R	-	-	-	-	-	0.25 to 2.0 mol% of V precursor
	O	-	-	-	-	-	1.0 mol %
	T	-	-	-	-	-	RR increases up to the optimum value then starts decreasing
Effect of scavengers and oxidant		-	-		-	-	94.2% at No scavenger 93.1% at $O_2^{-}\cdot$ scavenger 67.2% at $OH\cdot$ scavenger 49.7% at h^+ scavenger

Table 5(b) Comparative study on the effect of operating parameters on the photocatalytic performance of $CaTiO_3$

Parameter		Reference				
		25	26	27	28	This study
Photocatalyst		$CaTiO_3$ + g-C_3N_4	$CaTiO_3$ + g-C_3N_4	$CaTiO_3$	B+$CaTiO_3$ + 5 % wt graphene oxide (GO)	$CaTiO_3$
Effect of pH	R	-	-	-	3 to 12	2 to 10
	O	-	-	-	6.05	6
	T	90.81% at pH=3 76.38% at pH =6 44.44% at pH=10	-	-	MB RR increases up to the optimum value after that no significant change is observed	COD RR increases up to the optimum value after that it starts decreasing
Effect of irradiation time (h)	R	-	-	0 to 4	0.5 to 3	0 to 12
	O	-	-	3.33	3	8
	T	-	-	MB RR increases up to optimum value after that no significant improvement is observed	TOC RR increases with increase in irradiation time	COD RR increases up to optimum value after that no significant improvement is observed
Effect of light intensity/Illumination wavelength	R	-	-	-	-	11 to 33 W
	O	-	-	-	-	33 W
	T	0.25:1 weight ratio of g-C_3N_4: $CaTiO_3$ 47.01% at No light 77.57% at 150 W UVA light	RhB RR 50% under UV light 72% under visible light 97% under sunlight	-	-	COD RR increases with an increase in light intensity
Effect of catalyst dose	R	-	-	0.05, 0.1 and 0.3 g	-	0.66 to 5.34 g L^{-1}
	O	-	-	-	-	3.33 g L^{-1}
	T	68.34% at 0.10 g L^{-1} 99.02% at 0.30 g L^{-1}	-	87.1% at 0.05 g 89.4% at 0.1 g 97% at 0.3 g	74.9% at 0.5 g L^{-1} 98.3% at 2.5 g L^{-1}	COD RR increases up to optimum value after that no significant improvement is observed
Effect of initial concentration (IC) of pollutant	R	5 to 15 mg L^{-1}	-	10, 20 and 30 ppm	-	700, 16,000 and 40,000 mg L^{-1}
	O	-	-	-	-	-
	T	76.38% for distilled water 73.98% for drinking water 71.3% for tap water	-	89.4% at 10 ppm 96.4% at 20 ppm 97% at 30 ppm		COD RR decreases as IC increase

Table 5(b) Comparative study on the effect of operating parameters on the photocatalytic performance of $CaTiO_3$ (*continued*)

Parameter		Reference				
		25	26	27	28	This study
Effect of calcination temperature (CT) (°C)	R	-	-	-	-	600, 700 and 800
	O	-	-	-	-	600
	T	-	-	-	-	COD RR decreases as CT increase 84% at 600 °C 78% at 700 °C 72% at 800 °C
Effect of doping	R	-	-	-	1 to 15 % weight of GO	-
	O	-	-	-	5 wt% GO	-
	T	77.51% at 0.25:1 95.20% at 0.50:1 97.0% at 1:1 weight ratio of graphitic carbon nitride: $CaTiO_3$	39%@$CaTiO_3$ 97% @$CaTiO_3$+g-C_3N_4	-	MB degradation 10.1% @$CaTiO_3$ 31.3% @B+$CaTiO_3$ 75.8% at B+$CaTiO_3$+1 wt% GO 87.4% at B+$CaTiO_3$+5 wt% GO 82.3% at B+$CaTiO_3$+10 wt% GO 77.6% at B+$CaTiO_3$+15 wt% GO	-
Effect of scavengers and oxidant		76.38% at No scavenger 72.14% at EDTA-2Na scavenger 71.13% at IPA scavenger 18.13% at BQ scavenger	RhB RR No scavenger > IPA > TEA > BQ	-	87.4% at no scavenger 81.2% at HCO_3^- 70.2%@ NO_3^- 65.8% at SSO_4^{2-} 77.9% at Cl^-	77.12% at $CaTiO_3$ 67.5% at $CaTiO_3$+ HCO_3 60.13% at $CaTiO_3$+ Cl^- 86% at $CaTiO_3$ + H_2O_2

Conclusion

The use of various photocatalysts in environmental remediation has grown significantly over the past few years. Several pollutants, including organic and inorganic pollutants, dyes, personal and pharmaceutical waste, and pesticides, can be degraded and removed from wastewater using this method of treatment. Before implementing large-scale operations, it is important to optimize several parameters that either directly or indirectly influence the photocatalysis process, including the amount of light, irradiation time, pH, catalyst dose, initial concentration of contaminant, reaction temperature, doping, oxidants doses, and radical scavengers. In this work, the influence of operational parameters on the photocatalytic treatment of synthetic wastewater using $CaTiO_3$ is investigated, and the ideal operating parameters for actual wastewater treatment are determined. The findings show that 33W UV light, pH 6.0, 3.33 g L^{-1} $CaTiO_3$ dose, and 8 h of irradiation at room temperature provide $CaTiO_3$ highest photocatalytic performance. Under these conditions, the COD removal was 77 to 100% for initial COD concentrations ranging from 40,000 to 700 mg L^{-1}. By adding 0.01M of H_2O_2, the COD removal increased from 77.12% to 86%. The COD removal decreased from 77.12% to 67.50% or 60.13%, respectively, upon the addition of HCO_3^- or Cl^- anions. The $CaTiO_3$ can be utilized for the actual wastewater including sewage treatment plant effluent, industrial effluent, and leachate for photocatalytic treatment as the results are encouraging.

Reference

[1] Mishra, S., Sundaram, B. Efficacy of nanoparticles as photocatalyst in leachate treatment. Nanotechnology for Environmental Engineering, 2022, 7, 1–20.

[2] Lee, J., Perera, D., Glickman, T., Taing, L. Water-related disasters and their health impacts: A global review. Progress in Disaster Science 2020, 8, 100123.

[3] Gregorio, C., Lichtfouse, E. Advantages and disadvantages of techniques used for wastewater treatment. Environmental Chemistry Letters, 2018, 17, 1–11.

[4] El Din Mahmoud, A., Fawzy, M. Bio-based methods for wastewater treatment: Green sorbents, *In*: Ansari, A., Gill, S., Gill, R., Lanza, G., Newman, L. Phytoremediation. Springer, Cham., 2016, 209–238.

[5] Abbas, A., Guo, J.-S., Ping, L., Ya, P., Al-Rekabi, W. Review on landfill leachate treatments. American Journal of Applied Sciences, 2009, 6(4), 672–684.

[6] Hussain, A., Kumari, R., Ghosh Sachan, S., Sachan, A. Biological wastewater treatment technology: Advancement and drawbacks. Microbial Ecology of Wastewater Treatment Plants, 2021, 175–192.

[7] Nur, R., Che radzi, N., Hamid, K. Enhancement of biological approach and potential of Lactobacillus delbrueckii in decolorization of textile wastewater - A review. IOSR Journal of Environmental Science, Toxicology and Food Technology, 2014, 8, 6–10.

[8] Othman, N.H., Alias, N.H., Fuzil, N.S., Marpani, F., Shahruddin, M.Z., Chew, C.M., …, Ismail, A.F. A review on the use of membrane technology systems in developing countries. Membranes, 2021, 12(1), 30.

[9] Shilpa, M., Muthukumar, S., Baranidharan, S. Advanced oxidation process for leachate treatment: A critical review. In: Maulin, P.S., Sweta, P.B., Gunay, Y.T. An innovative approach of advanced oxidation processes for wastewater treatment, CRC Press, 2022.

[10] Shokri, A., Fard, M. A critical review in the features and application of photocatalysts in wastewater treatment. Chemical Papers, 2022, 76.

[11] Chanu, L.A., Singh, W.J., Singh, K., Nomita D.K. Effect of operational parameters on the photocatalytic degradation of methylene blue dye solution using Manganese doped ZnO nanoparticles. Results in Physics, 2018, 12, 1230–1237.

[12] Gusain, R., Kumar, N., Sinha, R., Suprakas. Factors influencing the photocatalytic activity of photocatalysts in wastewater treatment. *In*: Fosso-Kankeu, E., Pandey, S., Sinha Ray, S. Photocatalysts in advanced oxidation processes for wastewater treatment, 2020.

[13] Kulkarni, Dr-S., Zope, G., Goswami, A., Meshram, P. Factors affecting photocatalytic degradation of reactive Green-19 with CdO-TiO_2 nanocomposite. Advances in Environmental Technology, 2023, 3, 185–194.

[14] Mohit, K., Ganesh, S., Ravi, K.S., Ram, S.S., Ankur, V., Birendra, N.R. 2Effect of operating parameters on photocatalytic degradation of dyes by using graphitic carbon nitride. *In*: Maulin, S., Sushma, D., Jayashankar, D., Photocatalytic degradation of dyes, Elsevier, 2021, 23–43,

[15] Bona, D., Pengxiang, S., Lukas, B., Jun, L., Mingjun, R., Zhiwei, P., …, Boxin, Z. Photocatalytic activity of $CaTiO_3$ derived from roasting process of bauxite residue. Journal of Cleaner Production, 2020, 244, 118598,

[16] Ferrari-Lima, A., Germiniano, T., Savoia, J., Ganascim Marques, R., Ribeiro, V., Ueda, A.

$CaTiO_3$ Perovskite in the photocatalysis of textile wastewater. Ambiente e Agua - An Interdisciplinary Journal of Applied Science, 2019, 14, 1.

[17] Han, C., Liu, J., Yang, W., Wu, Q., Yang, H., Xue, X. Photocatalytic activity of CaTiO3 synthesized by solid state, sol–gel and hydro-thermal methods. Journal of Sol-Gel Science and Technology, 2016, 81(3), 806–813.

[18] Manjusha, P., Bonamali, P. A review on CaTiO3 photocatalyst: Activity enhancement methods and photocatalytic applications. Powder Technology, 2021, 388, 274–304.

[19] Zhang, D., Liu, S., Song, X., Xu, Z., Yang, B., Chen, L., …, Li, F. Preparation of calcium titanate based on the cotton template method and its simultaneous removal performance to heavy metals and organic pollutants in water. Journal of Advanced Oxidation Technologies. 2016, 19(1), 9–18.

[20] Xie, J., Ye, Q., Zhou, J., Liao, Y., Qian, G. The photocatalytic activity of $CaTiO_3$ derived from the microwave-melting heating process of blast furnace slag. Nanomaterials, 2023, 13, 1412.

[21] Gaikwad, S., Borhade, A., Gaikwad, V. A green chemistry approach for synthesis of $CaTiO_3$ photocatalyst: Its effects on degradation of methylene blue, phytotoxicity and microbial study. Der Pharma Chemica, 2012, 4, 184–193.

[22] Portia, S.A.U., Parthibavarman, M., Ramamoorthy, K. Unpredicted visible light induced advanced photocatalytic performance of Eu doped $CaTiO_3$ nanoparticles prepared by facile sol–gel technique. Journal of Cluster Science, 2022, 33, 2093–2102.

[23] Lu, X., Zhou, Q., Yin, H., Wang, A., Meng, F. Synthesis of hollow B-SiO_2@$CaTiO_3$ nanocomposites and their photocatalytic performance in ammonia nitrogen degradation. Water, Air, & Soil Pollution, 2020, 231, 102.

[24] Bantawal, H., Shenoy, S., Bhat, D. Vanadium doped $CaTiO_3$ cuboids: Role of vanadium in improving the photocatalytic activity. Nanoscale Advances, 2021, 3.

[25] Tuna, Ozlem. Construction of $CaTiO_3$/g-C_3N_4 heterostructure for boosting photodegradation of Indigo Carmine under visible light illuminationGorunur Isık Altında Indigo Karminin Fotodegradasyonunu Artırmak icin $CaTiO_3$/g-C3N4 Heteroyapısının Sentezlenmesi. International Journal of Advances in Engineering and Pure Sciences, 2023, 35.

[26] Kumar, A., Schurings, C., Kumar, S., Kumar, A., Krishnan, V. Perovskite-structured $CaTiO_3$ coupled with g-C_3N_4 as a heterojunction photocatalyst for organic pollutant degradation. Beilstein Journal of Nanotechnology, 2018, 9, 671–685.

[27] Karthikeyan, C., Thamima, M., Subbian, K. Dye removal efficiency of perovskite structured $CaTiO_3$ nanospheres prepared by microwave assisted method Peer-review under responsibility of the scientific committee of the Exploring Nanostructures for Enhanced Power Conversion Efficiency of Solar Cells Conference. Materials today: proceedings. 2019,

[28] Altin, I. Perovskite type B-$CaTiO_3$ coupled with graphene oxide as efficient bifunctional composites for environmental remediation. Processes, 2023, 11, 3191.

[29] Naveensubramaniam, V., Venkatraman, S., Imthiaz, S., Drweesh, E., Elnagar, M., Koppala, S., Swamiappan, S. Synthesis and characterization of calcium and magnesium based oxides and titanates for photocatalytic degradation of rhodamine B: A comparative study. Scientific Reports, 2023, 13.

[30] Garcна-Mendoza, M., Torres Ricardez, R., Ramirez Morales, E., Alvarez, J.G., Diaz, L., Del Angel, E., …, Perez-Hernandez, G. $CaTiO_3$ perovskite synthetized by chemical route at low temperatures for application as a photocatalyst for the degradation of methylene blue. Journal of Materials Science: Materials in Electronics, 2023, 34.

[31] Luo, M., Xu, J., Xu, W., Zheng, Y., Wu, G., Jeong, T. Photocatalytic activity of MoS2 nanoflower-modified $CaTiO_3$ composites for degradation of RhB under visible light. Nano-materials, 2023, 13, 636.

[32] Xin, Y., Xiaojun, H., Ying, F., Yahong, M., Zhenjun, W., Wensheng, L., …, Ligang, T. Synthesis of rodlike $CaTiO_3$ with enhanced charge separation efficiency and high photocatalytic activity. International Journal of Electrochemical Science, 2014, 9(9), 5155–5163.

[33] Azhar, A., Halim, A., Nazurah, N., Abidin, Z., Awang, N., Ithnin, A., …, Bin A Wahab, M. Ammonia and COD removal from synthetic leachate using rice husk composite adsorbent. Journal of Urban and Environmental Engineering, 2011, 5(1), 24-3124.

[34] Sundaram, B., Kumar, A. Long-term effect of metal oxide nanoparticles on activated sludge. Water Science & Technology, 2016, 75.

[35] Zhou, L., Zhuang, W.Q., Wang, X., Yu, K., Yang, S., Xia, S. New insights into comparison between synthetic and practical municipal waste-water in cake layer characteristic analysis of membrane bioreactor. Bioresource Technology, 2017, 244.

[36] Amakiri, K., Angelis-Dimakis, A., Ramirez-Canon, A. Recent advances, influencing factors, and future research prospects using photo-catalytic process for produced water treatment. Water Science & Technology, 2021, 85.

[37] Gnanaprakasam, A., Sivakumar, V.M. Thirumarimurugan, M. Influencing parameters in the photocatalytic degradation of organic effluent via nanometal oxide catalyst: A review. Indian Journal of Materials Science. 2015, 1–16.

[38] Tahir, M.B., Sohaib, M., Sagir, M., Rafique, M. Role of nanotechnology in photocatalysis. Reference Module in Materials Science and Materials Engineering, 2020.

[39] Subramaniam, M.N., Goh, P.-S., Lau, W.-J., Ng, B.-C., Ismail, A.F. Development of nanomaterial-based photocatalytic membrane for organic pollutants removal. Advanced Nanomaterials for Membrane Synthesis and Its Applications, 2019, 45–67.

[40] Jain, A., Vaya, D. Photocatalytic activity of TiO_2 nanomaterial. Journal of the Chilean Chemical Society, 2017, 62(4), 3683–3690.

[41] Galstyan, V., Comini, E., Faglia, G., & Sberveglieri, G. TiO_2 nanotubes: Recent advances in synthesis and gas sensing properties. Sensors (Basel, Switzerland), 2013, 13, 14813–14838.

[42] Suzuki, T., Kitahara, G., Arai, T., Matsuoka, Y., Morikawa, T. Nitrogen and transition-metal codoped titania nanotube arrays for visible-light-sensitive photoelectrochemical water oxidation. Chemical Communications (Cambridge, England), 2014, 50.

[43] Huang, K.C., Chien, S.H. Improved visible-light-driven photocatalytic activity of rutile/ titania-nanotube composites prepared by microwave-assisted hydrothermal process. Applied Catalysis B-Environmental, 2013, 140, 283–288.

[44] Li, X., Zhao, J., Yang, J. Semihydrogenated BN Sheet: A promising visible-light driven photocatalyst for water splitting. Scientific Reports, 2013, 3, 1858.

[45] Orawan, R., Thammasak, R., Sanya, S. Removal of color and chemical oxygen demand from landfill leachate by photocatalytic process with AC/TiO_2. Energy Procedia, 2015, 79, 536–541.

[46] Sama, A., Ayoub, K.-J., Sirus, J., Hamid, A. Photocatalytic treatment of landfill leachate using cascade photoreactor with immobilized W-C-codoped TiO_2 nanoparticles. Journal of Water Process Engineering, 2020, 36, 101307.

[47] Daneshvar, N., Rabbani, M., Modirshahla, N., Behnajady, M.A. Kinetic modeling of photocatalytic degradation of Acid Red 27 in UV/ TiO_2 process. Journal of Photochemistry and Photobiology A: Chemistry, 2004, 168(1–2), 39–45.

[48] Mondal, K., Sharma, A. Photocatalytic oxidation of pollutant dyes in wastewater by TiO_2 and ZnO nanomaterials–A mini-review. *In*: Ashok, M., Jayesh, R.B. Nanoscience & Technology for Mankind, 2014, 5, 36–72.

[49] Kumar, A., Pandey, G. A review on the factors affecting the photocatalytic degradation of hazardous materials. International Journal of Materials Science and Engineering, 2017, 1(3), 106–114.

[50] Sujatha, G., Shanthakumar, S., Chiampo, F. UV light-irradiated photocatalytic degradation of coffee processing wastewater using TiO_2 as a catalyst. Environments, 2020, 7, 47.

[51] Al-Nuaim, M.A., Alwasiti, A.A., Shnain, Z.Y. The photocatalytic process in the treatment of polluted water. Chemical Papers, 2023, 77, 677–701.

[52] Sinar Mashuri, S.I., Ibrahim, M.L., Kasim, M.F., Mastuli, M.S., Rashid, U., Abdullah, A.H., … Yun Hin, T.Y. Photocatalysis for organic wastewater treatment: From the basis to current challenges for society. Catalysts, 2020, 10(11), 1260.

[53] Jiao, Y., Han, D., Lu, Y., Rong, Y., Fang, L., Liu, Y., Han, R. Characterization of pine-sawdust pyrolytic char activated by phosphoric acid through microwave irradiation and adsorption property toward CDNB in batch mode. Desalination and Water Treatment, 2017, 77, 247–255.

[54] Hussein, F. Photochemical treatments of textile industries wastewater. Asian Journal of Chemistry, 2012, 24, 5427–5434.

[55] Reza, K.M., Kurny, A., Gulshan, F. Parameters affecting the photocatalytic degradation of dyes using TiO_2: A review. Applied Water Science, 2015, 7(4), 1569–1578.

[56] Azadi, S., Karimi-Jashni, A., Javadpour, S., Mahmoudian-Boroujerd, L. Photocatalytic landfill leachate treatment using P-type TiO_2 nanoparticles under visible light irradiation. Environment, Development and Sustainability, 2021, 23, 6047–6065.

[57] Carneiro, P.A., Umbuzeiro, G.D.A., Zanoni, M.V.B., Oliveira, D.P. Mutagenic activity removal of selected disperse dye by photoeletrocatalytic treatment. Journal of Applied Electrochemistry, 2010, 40(3), 485–492.

[58] Gaya, U.I., Abdullah, A.H. Heterogeneous photocatalytic degradation of organic contaminants over titanium dioxide: A review of fundamentals, progress and problems. Journal of Photochemistry and Photobiology C: Photochemistry Reviews, 2008, 9(1), 1–12.

[59] Anpo, M., Kamat, P.V. Environmentally benign photocatalysts: Applications of titanium oxide-based materials. New York: Springer, 2010.

[60] Andrade, M.A., Mestre, A.S., Carmona, R.J., Carvalho, A.P., Ania, C.O. Effect of the irradiation wavelength on the performance of nanoporous carbon as an additive to TiO_2. Applied Catalysis A: General, 2015, 507, 91–98.

[61] Chen, X., Wu, Z., Liu, D., Gao, Z. Preparation of ZnO photocatalyst for the efficient and rapid photocatalytic degradation of azo dyes. Nanoscale Research Letters, 2017, 12(1).

[62] Saikumari, N., Dev, S.M. Dev, S.A. Effect of calcination temperature on the properties and applications of bio extract mediated titania nano particles. Scientific Reports, 2021, 11, 1734.

[63] Kim, M., Kang, J., Lee, J., Kim, K.S., Kim, K., Cho, M., Lee, S.G. Effects of calcination temperature on the phase composition, photocatalytic degradation, and virucidal Activities of TiO_2 nanoparticles. ACS Omega, 2021, 6(16), 10668–10678.

[64] Shilpa, M., Pavan, K.N., Baranidharan, S. Effect of calcination temperature on structural, optical and photocatalytic properties of calcium titanate ($CaTiO_3$) nanoparticle. Results in Optics, 2024, 100676,

[65] Singh, G., Kaur Ubhi, M., Bedi, K., Singla, C. A Review on impacting parameters for photocatalytic degradation of organic effluents by ferrites and their nanocomposites. Processes 2023, 11, 1727.

[66] Yanda Shaba, E., Jacob, J., Tijani, J., Suleiman, M. A critical review of synthesis parameters affecting the properties of zinc oxide nanoparticle and its application in wastewater treatment. Applied Water Science, 2021, 11, 48.

[67] Shah, A., Rather, M. Effect of calcination temperature on the crystallite size, particle size and zeta potential of TiO_2 nanoparticles synthesized via polyol-mediated method. Materials Today: Proceedings, 2020, 44, 482–488.

[68] Mishra, S., Naini, P., Sundaram, B., Photocatalytic treatment of landfill leachate using $CaTiO_3$ nanoparticles. Environmental Nanotechnology, Monitoring & Management, 2023, 20, 100904.

[69] Mishra, S., Sundaram, B. A review of the photocatalysis process used for wastewater treatment. Materials Today: Proceedings, 2023.